OPEN

Oncogene (2017) **36**, 3673–3685

www.nature.com/onc

ORIGINAL ARTICLE

Characterization of PTEN mutations in brain cancer reveals that pten mono-ubiquitination promotes protein stability and nuclear localization

Jr-M Yang[1,4], P Schiapparelli[2,3,4,5], H-N Nguyen[1,4], A Igarashi[1,4], Q Zhang[1], S Abbadi[2], LM Amzel[3], H Sesaki[1], A Quinones-Hinojosa[2,3,5] and M Iijima[1]

PTEN is a PIP3 phosphatase that antagonizes oncogenic PI3-kinase signalling. Due to its critical role in suppressing the potent signalling pathway, it is one of the most mutated tumour suppressors, especially in brain tumours. It is generally thought that PTEN deficiencies predominantly result from either loss of expression or enzymatic activity. By analysing PTEN in malignant glioblastoma primary cells derived from 16 of our patients, we report mutations that block localization of PTEN at the plasma membrane and nucleus without affecting lipid phosphatase activity. Cellular and biochemical analyses as well as structural modelling revealed that two mutations disrupt intramolecular interaction of PTEN and open its conformation, enhancing polyubiquitination of PTEN and decreasing protein stability. Moreover, promoting mono-ubiquitination increases protein stability and nuclear localization of mutant PTEN. Thus, our findings provide a molecular mechanism for cancer-associated PTEN defects and may lead to a brain cancer treatment that targets PTEN mono-ubiquitination.

Oncogene (2017) **36,** 3673–3685; doi:10.1038/onc.2016.493; published online 6 March 2017

INTRODUCTION

The phosphatase and tensin homologue deleted from chromosome 10 (PTEN) is one of the most important tumour suppressor genes, and it is highly mutated in many types of cancers including brain, breast, kidney, lung and uterine cancers.[1–3] Many patients with brain tumours carry mutations in the PTEN genes.[1,4] Among these, glioblastoma (GBM), the most aggressive form that is associated by a short median prognosis (3 months without treatment), has a very high frequency of mutation (~35%) in the PTEN gene.[5,6] Importantly, PTEN deficiency in GBM has been associated with poor survival.[7,8] Treatments are currently limited: Despite extensive surgical resection, tumour recurrence is a common event and leads to a short median life expectancy (14.6 months) even with multimodal therapy that includes surgery, chemotherapy and radiotherapy.[9–11] Therefore, it is critical to elucidate mechanisms by which defects in PTEN function contribute to tumorigenesis in GBM, which can potentially serve as targets for treatment.

The PTEN protein is a lipid phosphatase that converts the tumorigenic lipid signal, phosphatidylinositol 3,4,5-trisphosphate (PIP3), to phosphatidylinositol 4,5-bisphosphate (PIP2) at the plasma membrane in cells. The majority of PTEN is located in the cytosol, and only a fraction is recruited to the plasma membrane to precisely control PIP3 levels in a highly regulated manner. We have previously shown that this recruitment process is mediated by the membrane-binding regulatory interface and is regulated by phosphorylation of PTEN.[12–15] The membrane-binding regulatory interface consists of three regions of PTEN and is located on the protein's surface. The phosphorylated C-terminal region of PTEN tightly binds to the interface and masks its access to the membrane. Upon dephosphorylation, the C-terminal tail dissociates from the membrane-binding regulatory interface and opens the conformation of PTEN, allowing it to interact with the membrane, thereby converting PIP3 to PIP2. In addition to this recruitment, opening the PTEN conformation stimulates its translocation to the nucleus, where PTEN functions in DNA repair and genome stability are likely independent of its lipid phosphatase activity.[16] Consistent with the function of the C-terminal region as a determinant of stability and nuclear translocation of PTEN, deletion of this region increases interaction of PTEN with E3 ligases NEDD4 that leads both mono- and polyubiquitylation on PTEN at the same residues K13 and K289. However, whether mono- and polyubiquitylation on PTEN compete and how these modifications are regulated remain unclear.

We further found that this membrane recruitment mechanism is defective in several cancer-associated mutations.[14] When we examined the PTEN mutations that did not affect its enzymatic activity, they specifically blocked the recruitment of PTEN to the plasma membrane. Forced tethering of these PTEN mutants to the plasma membrane using an artificial membrane anchor restored their ability to oppose tumorigenic PIP3 signalling even in the presence of cancer-associated mutations. Thus, our findings have shown the importance of regulated PTEN-membrane interactions

[1]Department of Cell Biology, Johns Hopkins University School of Medicine, Baltimore, MD, USA; [2]Department of Neurosurgery, Johns Hopkins University School of Medicine, Baltimore, MD, USA and [3]Department of Biophysics and Biophysical Chemistry, Johns Hopkins University School of Medicine, Baltimore, MD, USA. Correspondence: Dr A Quiñones-Hinojosa, Department of Neurosurgery, Mayo Clinic College of Medicine, 4500 San Pablo Rd., Jacksonville, FL 32224, USA or Dr M Iijima, Department of Cell Biology, Johns Hopkins University School of Medicine, 725N. Wolfe Street, 107 Hunterian, Baltimore, MD 21205, USA.
E-mail: Quinones-Hinojosa.Alfredo@mayo.edu or miijima@jhmi.edu
[4]These authors contributed equally to this work.
[5]Present address: Department of Neurosurgery, Mayo Clinic College of Medicine, Jacksonville, FL, USA.
Received 16 May 2016; revised 21 November 2016; accepted 29 November 2016; published online 6 March 2017

in the tumour suppressor function of PTEN in cancers. These findings suggest that cancer-related defects in PTEN go beyond its loss of expression and inactivation of its enzymatic activity; however, the landscape of PTEN defects in human cancers remains unknown.

To investigate the spectrum of cancer-related PTEN defects, we established 17 primary cells derived from 16 GBM patients and analysed their PTEN mutations, expressions, activities and membrane localizations. We revealed an unforeseen high occurrence of amino acid substitutions that blocked localization of PTEN at the plasma membrane and nucleus, but not its enzymatic activity. These mutations were found to alter the architecture of the membrane-binding regulatory interface, leaving the protein conformation open while inactivating mechanisms that target the membrane and nucleus. This abnormally opened PTEN is subject to polyubiquitination, and therefore increased degradation. Toward rescuing these cancer-linked proteins, we show that increasing mono-ubiquitination can stabilize them and redistribute them to the nucleus.

RESULTS

Analysis of PTEN mutations in malignant GBM cells

Using both immunoblotting with antibodies to PTEN and RT-PCR (Figures 1a–c), we examined the PTEN protein in cells obtained from 16 GBM patients. Primary human fetal neural stem cells from two embryos were used as controls.[17–21] Primary cells obtained from nine patients (GBMs 612, 626, 651, 832, 965, 549, 922, 963 and 854) showed undetectable amounts of PTEN proteins. Of these, three (GBMs 612, 626 and 832) showed no detectable signals in an RT-PCR assay, suggesting defects in chromosomes, transcription or mRNA stability. Six expressed mRNA, and of these, four showed PTEN with non-sense mutations (GBMs 965 and 549), in-frame deletion of exon 3 (GBM 922), or out-of frame deletion of exon 4 (GBM 854). Interestingly, one (GBM 963) had no mutations in PTEN cDNA, yet lost protein expression, suggesting that the translation or stability of PTEN was altered by mutations in the non-coding region of PTEN or in other genes. Of eight patient cells that showed expression of PTEN, six (GBMs 640, 153, 940, 911, 944 and 960) contained wild-type PTEN; GBM in these patients is unlikely caused by PTEN deficiency. Two cells (GBMs 847 and 922) were derived from the same patient at different times (primary and recurrent tumour) and showed a truncated PTEN caused by deletion of exon 3.

We found two cells, GBMs 651 and 276, each of which contained a previously uncharacterized point mutation in the PTEN coding region. The former carried L320S while the latter carried T277A. Both mutant proteins had decreased steady state levels and were located at the junction where the phosphatase and C2 domains are connected in the crystal structure of PTEN (Figure 1d). We have previously shown that these two domains form the membrane-binding regulatory interface that binds to the plasma membrane as well as the inhibitory phosphorylated C-terminal tail, creating a master switch to determine PTEN localization.[14] We focused on the molecular mechanisms by which L320S and T277A block PTEN function.

$PTEN_{L320S}$ and $PTEN_{T277A}$ are enzymatically active

Because most cancer-associated mutations in PTEN abolish its essential phosphatase activity, we first tested whether L320S and T277A affect enzymatic activity. We immunopurified GFP fused to $PTEN_{L320S}$ and $PTEN_{T277A}$, wild-type PTEN ($PTEN_{WT}$), a catalytically inactive $PTEN_{C124S}$, and PTEN with a deletion of exon 3 ($PTEN_{delEx3}$) from HEK293T cells. Equal amounts of immunopurified proteins were used to measure their lipid phosphatase activity against a PIP3 substrate *in vitro*.[15,22] While $PTEN_{C124S}$-GFP and $PTEN_{delEx3}$-GFP showed significantly suppressed lipid phosphatase activities, $PTEN_{L320S}$-GFP and $PTEN_{T277A}$-GFP showed activities indistinguishable from $PTEN_{WT}$-GFP (Figure 1e).

$PTEN_{L320S}$ and $PTEN_{T277A}$ have reduced activity to suppress PIP3 signalling

To test whether ectopic expression of PTEN can suppress PIP3 signalling in patient-derived GBM cells, we introduced $PTEN_{WT}$-GFP into GBM 651 (which expressed $PTEN_{L320S}$), GBM 965 (which expressed no PTEN proteins) and GBM 276 (which expressed $PTEN_{T277A}$). Immunoblotting of whole lysates showed that $PTEN_{WT}$-GFP significantly decreased phosphorylated AKT levels in all three GBM cells (Figures 1f and g). Taking advantage of this expression system, we further tested the function of PTEN mutants in the PTEN-null GBM cell GBM 965. Steady state levels of $PTEN_{T277A}$-GFP, $PTEN_{L320S}$-GFP and $PTEN_{delEx3}$-GFP were significantly lower than that of $PTEN_{WT}$-GFP (Figures 1h and i). When we measured AKT phosphorylation, a key signalling event downstream of PIP3 signalling, $PTEN_{WT}$ decreased it by more than 80% in the PTEN-null GBM 965 cells. In contrast, $PTEN_{L320S}$ and $PTEN_{delEx3}$ showed decreased activity to suppress AKT phosphorylation (Figure 1j). We also examined whether PTEN expression inhibits cell migration and proliferation, both of which are stimulated by PIP3. $PTEN_{L320S}$-GFP, $PTEN_{T277A}$-GFP and $PTEN_{delEx3\text{-}GFP}$ showed decreased activity to suppress cell migration, as measured by the Transwell (Figure 1k) or 3-D nanopattern migration assays[23–25] (Figure 1l). Similarly, $PTEN_{L320S}$-GFP, and $PTEN_{T277A}$-GFP and $PTEN_{delEx3}$-GFP were unable to effectively rescue cancer cell proliferation, compared to $PTEN_{WT}$-GFP (Figure 1m).

Consistent with data obtained in GBM cells, unlike $PTEN_{WT}$-GFP, $PTEN_{L320S}$-GFP expression did not effectively suppress phospho-AkT levels in HEK293T cells, nor did $PTEN_{C124S}$-GFP and $PTEN_{delEx3}$-GFP (Figures 2a and b). $PTEN_{T277A}$-GFP slightly decreased phospho-AKT levels, though to a lesser extent than $PTEN_{L320S}$-GFP. Expression levels of $PTEN_{delEx3}$-GFP, $PTEN_{L320S}$-GFP and $PTEN_{T277A}$-GFP were significantly lower than those of $PTEN_{WT}$-GFP or $PTEN_{C124S}$-GFP (Figures 2a and b), suggesting that lower protein levels might contribute to the inability of these mutant proteins to effectively suppress AKT phosphorylation. To determine if lower levels of these three fused proteins result from

Figure 1. Identification of PTEN mutations in GBM cells. (**a**) Protein and mRNA analyses of PTEN in GBM samples. Whole cell lysates were analysed using SDS-PAGE and immunoblotting with antibodies to PTEN and actin. PTEN mRNA transcripts were analysed using RT-PCR. GAPDH was the control. (**b**) A summary of PTEN mutations found in 17 patient-derived GBM cells. Two human fetal neural stem cells were controls. (**c**) Distribution of various types of PTEN mutations in GBM cells. (**d**) Locations of exon 3, T277 and L320 (red) in the PTEN 3-D structure.[35] (**e**) Phosphatase activity of PTEN mutants purified from HEK293T cells as measured by the amount of phosphate released from PIP3 diC8 per minute using the malachite green assay. Values represent mean ± s.e.m. ($n \geq 3$). (**f**) GFP or $PTEN_{WT}$-GFP were expressed in the indicated GBM cells. Their whole cell lysates were subjected to immunoblotting. (**g**) Quantification of AKT phosphorylation. Values represent mean ± s.e.m. ($n = 3$). (**h**) Various PTEN-GFP constructs were expressed in the PTEN-null GBM cell GBM 965. Whole cell lysates were analysed by immunoblotting. PTEN steady state levels (**i**) and AKT phosphorylation (**j**) were quantified. Values represent mean ± s.e.m. ($n = 3$). The GBM 965 cell expressing various PTEN constructs were analysed for cell migration by Transwell (**k**) and nanopattern cell migration (**l**) assays. In the nanopatten cell migration assay, more than 150 cells were analysed in each experiment ($n = 3$ experiments). (**m**) GBM 965 cells expressing indicated PTEN constructs were analysed for cell proliferation on day 7 after seeding ($n = 3$).

reduced synthesis or stability, we measured their half-lives by blocking protein synthesis; this was done with cycloheximide in the human GBM cell line U87MG, the human breast basal epithelial cell line MCF10A, which lacks PTEN and HEK293T cells (Figures 2d and e and S1A). We found that $PTEN_{delEx3}$, $PTEN_{L320S}$ and $PTEN_{T277A}$ had significantly shorter half-lives than $PTEN_{WT}$ or $PTEN_{A4}$, which carries alanine substitutions at S380, T382, T383 and S385 that block phosphorylation of C-terminal tail,[15,22] (Figures 2d and e). Therefore, $PTEN_{delEx3}$, $PTEN_{L320S}$ and $PTEN_{T277A}$ undergo accelerated degradation.

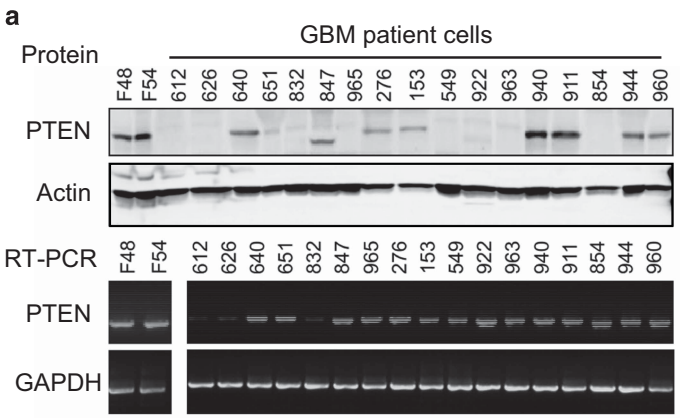

b

Sample ID	Gender	Age	Protein	mRNA/mutation
GBM612	M	56	No	No
GBM626	M	53	No	No
GBM640	F	60	Yes	WT
GBM651	M	59	No	L320S
GBM832	F	61	No	No
GBM847	F	50	Small	Deletion of Exon 3
GBM965	F	61	No	R335stop
GBM276	F	53	Yes	T277A
GBM153	F	69	Yes	WT
GBM549	F	83	No	K144stop
GBM922	F	51	No	Deletion of Exon 3
GBM963	F	64	No	WT
GBM940	M	47	Yes	WT
GBM911	M	24	Yes	WT
GBM854	F	41	No	Deletion of Exon 4
GBM944	M	53	Yes	WT
GBM960	M	75	Yes	WT
F48	-	18-20 wk	Yes	WT
F60	-	18-20 wk	Yes	WT

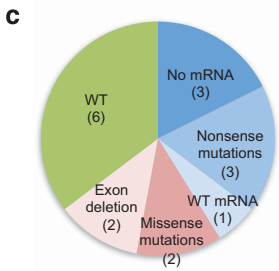

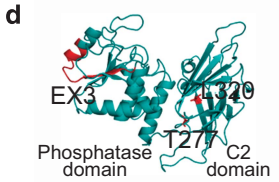

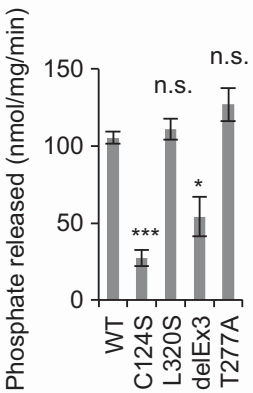

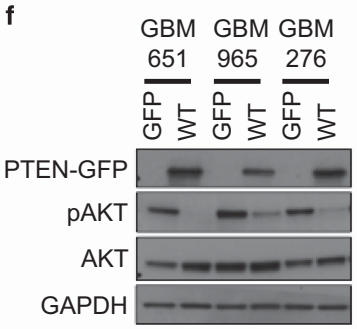

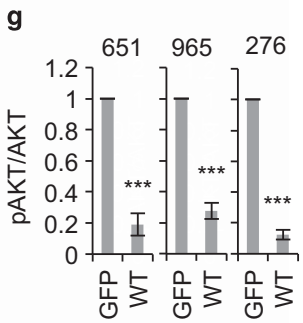

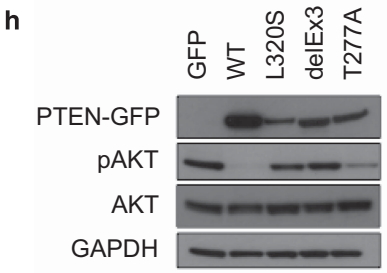

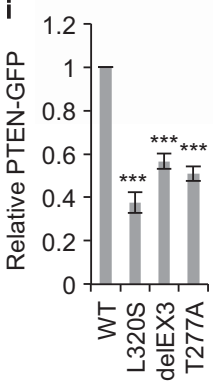

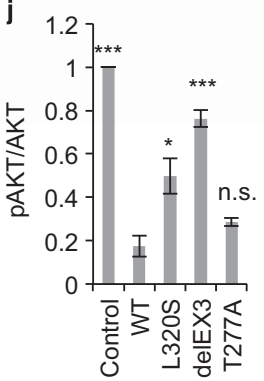

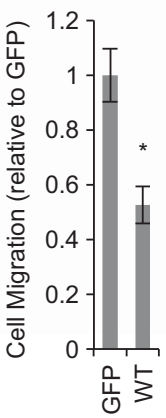

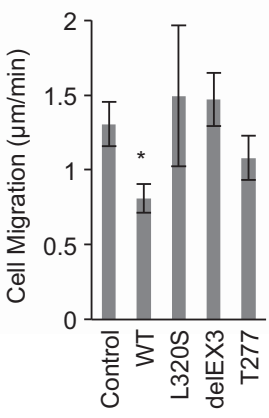

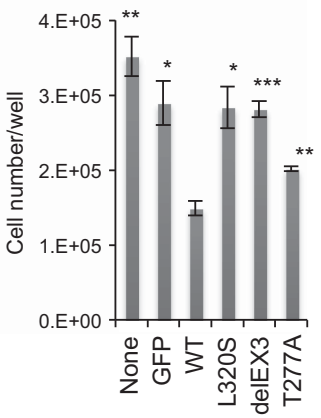

$PTEN_{L320S}$ cannot be stabilized by removing known destabilizing modifications in PTEN

To determine the mechanism that decreases the stability of $PTEN_{L320S}$ in greater detail, we combined L320S with mutations that are known to increase PTEN stability. We introduced K13R, which has been shown to block ubiquitination at K13, a cause of proteasomal degradation, and C124S, a mutation that stabilizes PTEN presumably through inhibiting its enzymatic activity.[12,13,15]

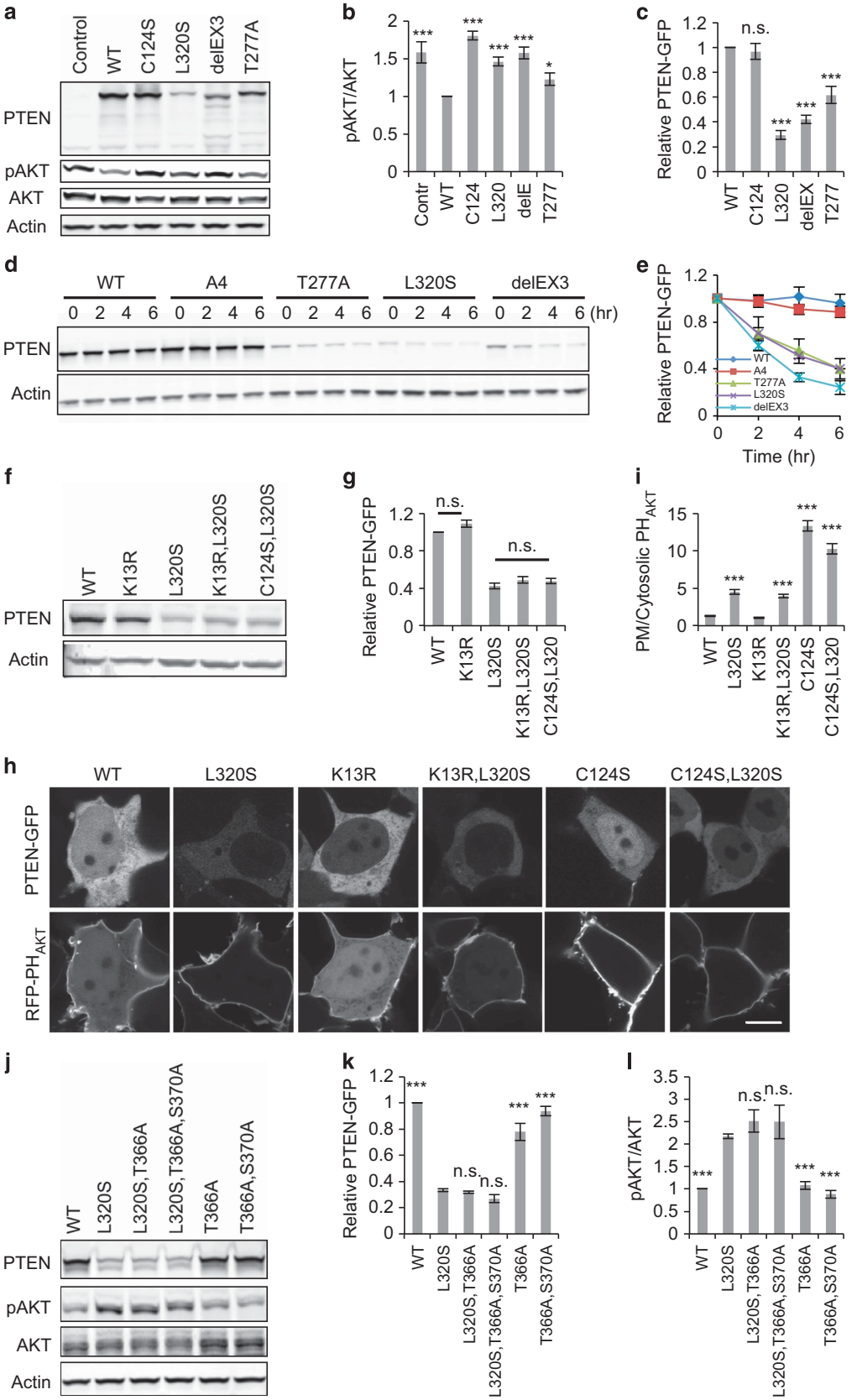

We found that neither of these two mutations rescued the stability of $PTEN_{K13R,L320S}$-GFP or $PTEN_{C124S,L320S}$-GFP (Figures 2f and g). Similarly, live-cell imaging showed that fluorescence intensity was not greater in $PTEN_{K13R,L320S}$-GFP or $PTEN_{C124S,L320S}$-GFP than in $PTEN_{L320S}$-GFP (Figures 2h and i). Consistent with these observations, $PTEN_{K13R,L320S}$-GFP did not decrease PIP3 levels, as revealed by the PIP3 biosensor RFP-PH_{AKT}. Interestingly, the membrane-bound portion of RFP-PH_{AKT} was 3-fold greater in $PTEN_{C124S}$-GFP-expressing cells than in $PTEN_{L320S}$-GFP-expressing cells, suggesting a dominant negative effect of $PTEN_{C124S}$ on endogenous PTEN phosphatase function, consistent with previous research.[26] We noticed that $PTEN_{C124S}$-GFP showed modestly more association with the plasma membrane than did $PTEN_{WT}$-GFP, consistent with previous studies;[27] however, $PTEN_{C124S,L320S}$-GFP was dissociated from the plasma membrane (Figure 2h), further supporting that L320S decreases interactions of PTEN with the plasma membrane.

It has been shown that phosphorylation of PTEN at T366 or S370 destabilizes the protein.[28,29] To determine whether blocking phosphorylation at these two sites increases the stability of $PTEN_{L320S}$, we created $PTEN_{L320S,T366A}$ and $PTEN_{L320S,T366A,S370A}$. Immunoblotting showed that $PTEN_{L320S}$-GFP, $PTEN_{L320S,T366A}$-GFP and $PTEN_{L320S,T366A,S370A}$-GFP were as unstable as $PTEN_{L320S}$-GFP (Figures 2j and k). These three constructs consistently failed to decrease AKT phosphorylation levels (Figures 2j and l).

Low cellular PTEN phosphatase activity by GBM mutants does not result solely from their lower steady state levels

When we examined intracellular localization of PTEN mutants using fluorescence microscopy, $PTEN_{delEx3}$-GFP, $PTEN_{L320S}$-GFP and $PTEN_{T277A}$-GFP showed uniform distributions in the cytosol, similar to that seen of $PTEN_{WT}$-GFP, although the overall fluorescence intensity of the three mutants was lower than that of $PTEN_{WT}$-GFP (Figure 3a). The PM/cytosolic fluorescence ratio of GFP fused to wild-type or mutant PTENs was not affected by amounts of their expression (data not shown). Consistent with immunoblotting using anti-phospho-AKT antibodies, quantitative live-cell imaging using a PIP3 biosensor, RFP-PH_{AKT}, which specifically binds to PIP3 in the plasma membrane, showed that expression of $PTEN_{WT}$-GFP greatly reduced PIP3 levels. This was measured by comparing the PM/cytosolic ratio of PH_{AKT} (RFP-PH_{AKT} intensity at the plasma membrane relative to that in the cytosol) to that of PTEN-GFP in HEK293T cells (Figure 3b). $PTEN_{T277A}$-GFP also decreased PIP3 levels, though not as strongly as did $PTEN_{WT}$-GFP (Figures 3a and b). $PTEN_{L320S}$-GFP and the enzymatically inactive $PTEN_{delEx3}$-GFP did not decrease PIP3 levels (Figures 3a and b). To determine whether protein expression levels contribute to the effect of wild-type and mutant PTEN-GFP on PIP3 levels, we quantified total GFP intensity and plotted it against the PM/cytosolic fluorescence ratio of PH_{AKT} for individual cells (Figure 3c). At comparable expression levels, $PTEN_{delEx3}$-GFP, $PTEN_{L320S}$-GFP and $PTEN_{T277A}$-GFP had weaker suppression of PIP3 levels than $PTEN_{WT}$-GFP (Figure 3c). Among the mutants, $PTEN_{T277A}$-GFP induced the strongest decrease in PIP3 levels, consistent with the effect of phospho-AKT. Thus, in these three cases, lower expression level alone does not account for the inability to effectively reduce PIP3.

L320S and T277A mutations block PTEN membrane and nuclear localization

The recruitment of PTEN to the plasma membrane is crucial for PTEN activity.[13] To determine the impact of the T277A and L320S mutations on PTEN membrane localization, we introduced T277A into $PTEN_{A4}$, $PTEN_{K13R,A4}$ and ePTEN, all of which are strongly recruited to the plasma membrane.[13] The use of the A4 mutation is critical to unambiguously determine the association of PTEN with the plasma membrane and nucleus as wild-type PTEN is predominantly cytoplasmic (Figure 4a).[14] We found that introducing T277A into $PTEN_{A4}$-GFP, $PTEN_{K13R,A4}$-GFP and ePTEN-GFP blocked membrane localization in all cases, leaving the fused proteins in the cytosol, in HEK293T cells (Figures 4a and b). Additionally, introducing the T277A mutation decreased the steady state levels of $PTEN_{A4}$, $PTEN_{K13R,A4}$ and ePTEN (Figures 4d and e) and their abilities to reduce AKT phosphorylation (Figures 4d and f). We observed similar inhibitions of membrane localization by L320S in $PTEN_{L320S,A4}$-GFP and $PTEN_{L320S,K13R,A4}$-GFP in HEK293T cells (Figures 4g and h) as well as U87MG cells and MCF10A cells lacking PTEN (Supplementary Figure S1B). Interestingly, both T277A and L320S inhibited nuclear accumulation of $PTEN_{A4}$-GFP (Figures 4a, c, g and i). The nuclear localization defects caused by T277A and L320S could further affect PTEN function in suppressing tumour formation, as nuclear PTEN has been implicated in chromosome stability, DNA repair and cell cycle progression.[16,30–32] When we compared the localization of these PTEN mutants with different expression levels, consistent localization was observed regardless their amounts (data not shown), therefore impaired localization does not result from differences in their abundance.

We have previously shown that artificial tethering of PTEN to the plasma membrane restores function of PTEN mutants, which are defective in their association with the plasma membrane.[14] To understand whether forced membrane tethering of $PTEN_{L320S}$ rescues its defects in PIP3 signalling, we added a myristoylation sequence, derived from the plasma membrane protein PKBR1[33] to the N-terminus of $PTEN_{L320S}$ (Myr-$PTEN_{L320S}$). The lipid anchor sequence increased the localization of Myr-$PTEN_{L320S}$-GFP to the plasma membrane, as revealed by fluorescence microscopy (Figures 4j and k). Coexpression of RFP-PH_{AKT} revealed a significant improvement of Myr-$PTEN_{L320S}$-GFP to help remove PIP3 in the plasma membrane (Figures 4j and l). These data suggest that the defect of $PTEN_{L320S}$ in PIP3 signalling partially results from decreased membrane association.

$PTEN_{L320S}$ does not induce phosphorylation or change phosphorylation of adjacent amino acids

Protein phosphorylation prediction analysis suggested that the substitution of L320 to S creates a new potential phosphorylation site (Supplementary Figure S2). We tested whether changing L320 to phospho-mimetic (L320D or L320E) or phospho-defective (L320A) amino acids affects the stability, localization or function of PTEN. Immunoblotting (Figure 5a) and live-cell imaging (Figure 5b) showed that neither the phospho-mimetic $PTEN_{L320D}$ or $PTEN_{L320E}$ nor the phospho-defective $PTEN_{L320A}$ showed instabilities similar to that seen in $PTEN_{L320S}$. In addition, introducing L320A into $PTEN_{A4}$ to produce $PTEN_{L320A,A4}$ did not

Figure 2. Stability of PTEN mutants. (**a**) Immunoblotting of whole cell lysates prepared from HEK293T cells expressing the indicated PTEN molecules fused to GFP. (**b**) Quantification of AKT phosphorylation. Values represent mean ± s.e.m. ($n = 5$). (**c**) Quantification of PTEN. Values represent mean ± s.e.m. ($n = 5$). (**d**) Human GBM U87MG cell lysates expressing various PTEN constructs were prepared at the indicated time points after addition of cycloheximide and analysed by immunoblotting with antibodies to PTEN and actin. (**e**) Quantification of PTEN levels after cycloheximide addition. Values represent mean ± s.e.m. ($n = 3$). (**f–h**) HEK293T cells expressing various PTEN mutants were quantitatively analysed by immunoblotting (**f, g**) and fluorescence microscopy (**h**). Values represent mean ± s.e.m. ($n = 6$). (**h, i**) PIP3 levels in cells were quantified using the membrane intensity of the PIP3 biosensor RFP-PH_{AKT}. Values represent mean ± s.e.m. ($n = 20$). (**j–l**) Whole cell lysates of HEK293T cells expressing various PTEN mutants were analysed by immunoblotting (**j, k**), and AKT phosphorylation (**j, l**) were quantified. Values represent mean ± s.e.m. ($n = 3$).

affect the strong inhibition of membrane and nuclear localization (Figure 5d). Finally, mass spectrometry showed that $PTEN_{L320S}$ was not phosphorylated at residue 320 (0 out of 82 L320S-containing peptides; Supplementary Figure S2). These data suggest that phosphorylation at residue 320 of $PTEN_{L320S}$ does not contribute to the defects in protein stability and localization.

We then tested whether L320S affects phosphorylation at other sites on PTEN. Two residues next to L320S, T319 and T321, have reportedly been phosphorylated by RhoA-associated kinase (ROCK) to promote PTEN membrane targeting[2,34] (Figure 5c). We found that introducing T319A and T321A mutations into $PTEN_{L320S}$ does not enhance protein stability (Figure 5d). Consistent with this, treating cells with the ROCK inhibitor Y-27632 showed no effect on $PTEN_{L320S}$ level (Figure 5d). Furthermore, T319A and T321A mutations did not enhance membrane localization of $PTEN_{L320S,A4}$-GFP (Figure 5e). Our data suggest that phosphorylation at nearby residues T319 and T321 has no role in controlling protein stability and localization of $PTEN_{L320S}$.

T277A and L320S open the conformation of PTEN and promote ubiquitination

The crystal structure of PTEN has shown that F273 interacts with L320.[35] We hypothesize that the interactions with this amino acid is necessary to stabilize PTEN conformation (Figure 5f). We found that an F273A mutation showed an inhibition similar to that of L320S, though milder, on both nuclear accumulation of $PTEN_{A4}$ and membrane localization of $PTEN_{K13R,A4}$ (Figures 5g and h). Our results suggest that an L320–F273 interaction plays an important role in maintaining the PTEN conformation that is necessary for localization at the plasma membrane and nucleus. Supporting this, swapping amino acid residues at 273 and 320 restored the localization of PTEN and $PTEN_{A4}$ in $PTEN_{F273L,L320F}$-GFP and $PTEN_{F273L,L320F,A4}$-GFP, respectively (Figure 5i).

To determine the effect of L320S and T277A on the protein conformation and folding of PTEN, we performed a trypsin digestion assay.[36] We immunopurified $PTEN_{WT}$-GFP, $PTEN_{A4}$-GFP, $PTEN_{T277A}$-GFP and $PTEN_{L320S}$-GFP from HEK293T cells and incubated them with various concentrations of trypsin at 37 °C. PTEN was analysed using SDS-PAGE followed by immunoblotting with anti-PTEN antibodies. Consistent with the open conformation of $PTEN_{A4}$,[15,36] we found greater susceptibility of $PTEN_{A4}$-GFP than of $PTEN_{WT}$-GFP to trypsin digestion (Figures 7a and b). As with $PTEN_{A4}$-GFP, both $PTEN_{T277A}$-GFP and $PTEN_{L320S}$-GFP showed lower half-lives of full-length GFP fusions during trypsin digestion (Figures 6a and b). Importantly, fragmentation patterns of $PTEN_{T277A}$ and

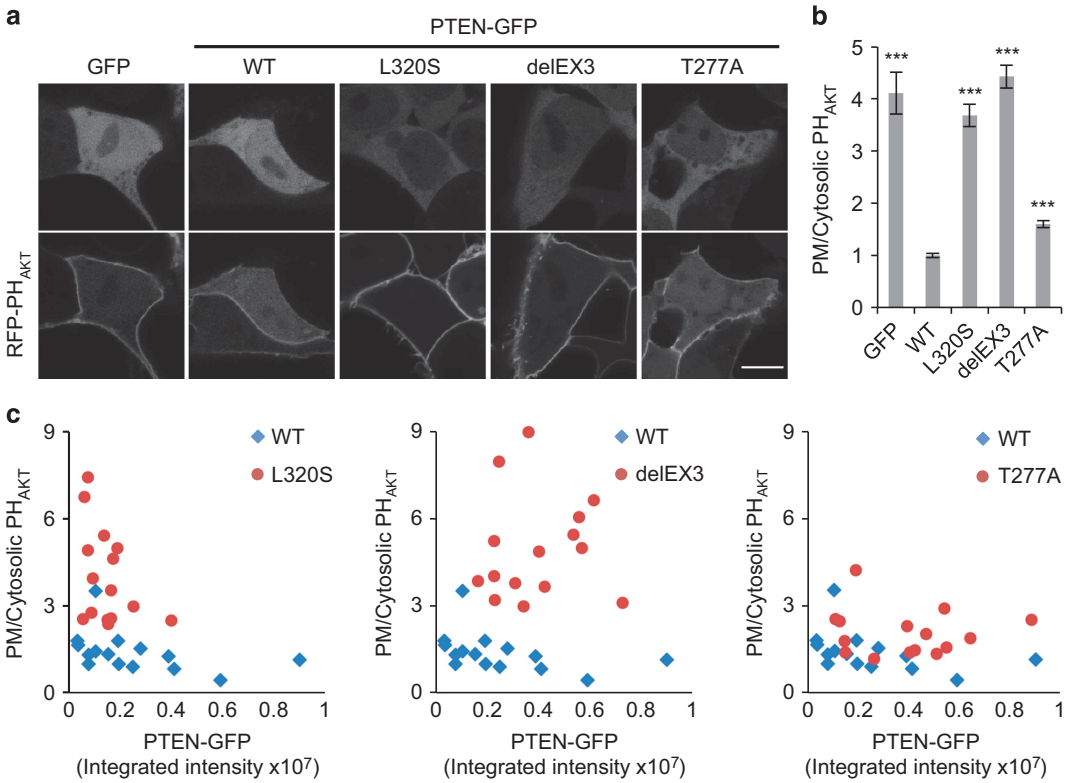

Figure 3. $PTEN_{L320S}$ and $PTEN_{T277A}$ show decreased activities to suppress PIP3 signalling. (**a**) HEK293T cells expressing GFP fused to the indicated PTEN molecules were examined using fluorescence microscopy. (**b**) Quantification of the membrane-associated PIP3 level using the PIP3 biosensor RFP-PH_{AKT}. Fluorescence intensity was measured as the ratio between membrane intensity and cytosol intensity.[37] Values represent mean ± s.e.m. ($n = 20$). (**c**) Correlations between total PTEN-GFP level and the membrane-bound RFP-PH_{AKT} fraction in HEK293T cells expressing $PTEN_{WT}$-GFP, $PTEN_{L320S}$-GFP, $PTEN_{delEx3}$-GFP, and $PTEN_{T277A}$-GFP ($n = 15$ for each PTEN-GFP protein).

Figure 4. Both T277A and L320S mutations inhibit membrane and nuclear localization of PTEN. (**a, g**) HEK293T cells expressing the indicated PTEN molecules were examined using fluorescence microscopy. (**b**, **c**, **h**, **i**) Quantification of PTEN accumulating at the plasma membrane (B and H) and nucleus (**c, i**). Values represent mean ± s.e.m. ($n = 20$). (**d**) Immunoblot analysis of HEK293T cells expressing various PTEN plasmids with the indicated antibodies. (**e, f**) Quantification of PTEN levels (**e**) and AKT phosphorylation (**f**). Values represent mean ± s.e.m. ($n = 3$). (**j**) HEK293T cells expressing GFP fused to the indicated PTEN molecules and RFP-PH_{AKT} were examined using fluorescence microscopy. (**b**) Quantification of the membrane-associated PTEN (**k**) and RFP-PH_{AKT} (**l**). Values represent mean ± s.e.m. ($n = 15$).

$PTEN_{L320S}$ are similar to each other, but distinct from that of $PTEN_{A4}$. Therefore, $PTEN_{T277A}$ and $PTEN_{L320S}$ have similar protein folding that are different from that of $PTEN_{A4}$.

To determine whether the altered protein conformations of $PTEN_{T277A}$ and $PTEN_{L320S}$ change the ubiquitination of PTEN, we co-expressed HA-ubiquitin with various GFP-PTEN constructs.

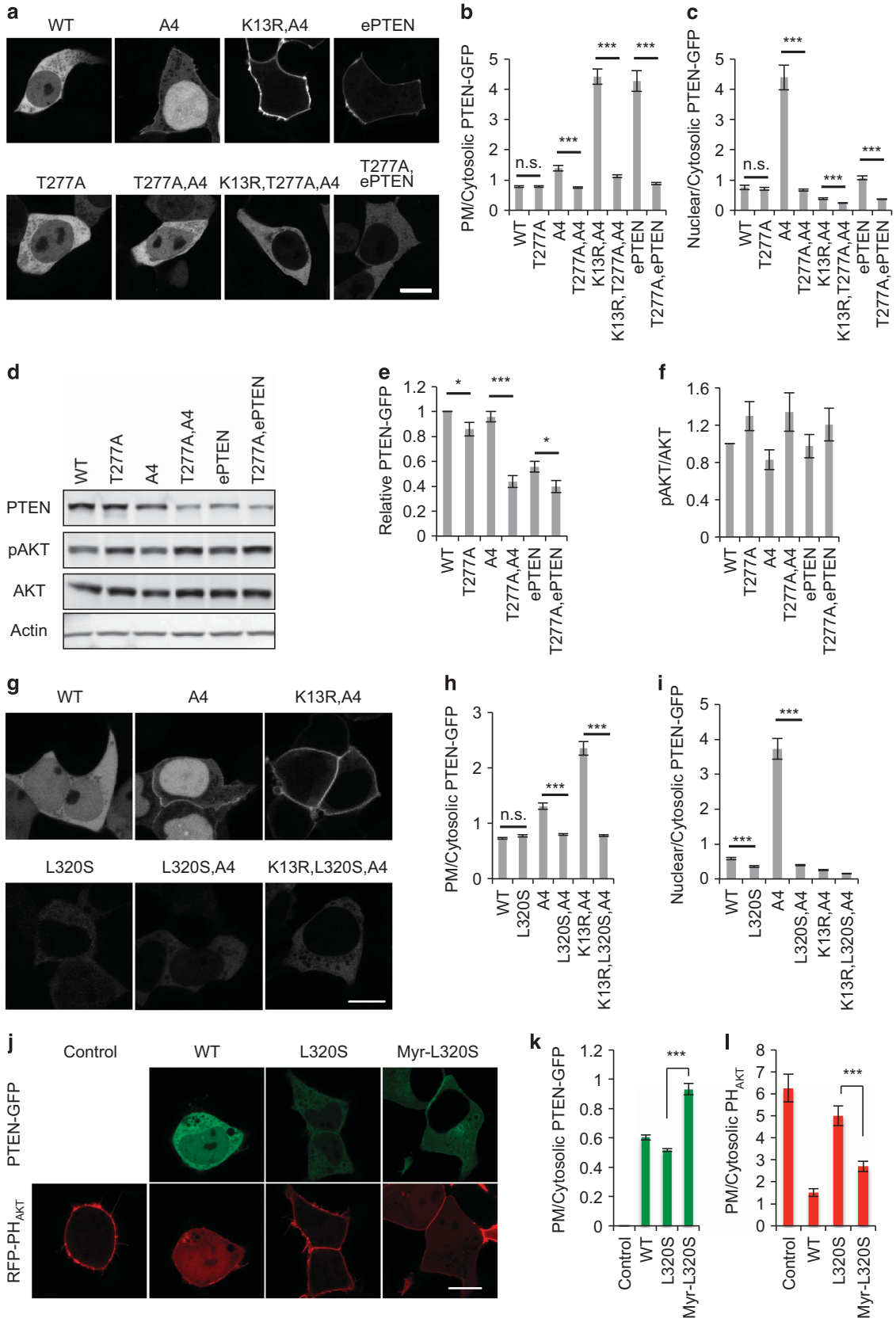

GFP fusions were immunoprecipitated and analysed for ubiquitination by immunoblotting with anti-HA antibodies. We found that opening the protein conformation in $PTEN_{A4}$ increased PTEN ubiquitination over that of $PTEN_{WT}$ (Figure 6c). As with $PTEN_{A4}$, both $PTEN_{T277A}$ and $PTEN_{L320S}$ showed increased ubiquitination. Combinations of these mutations with A4 appear not to additionally

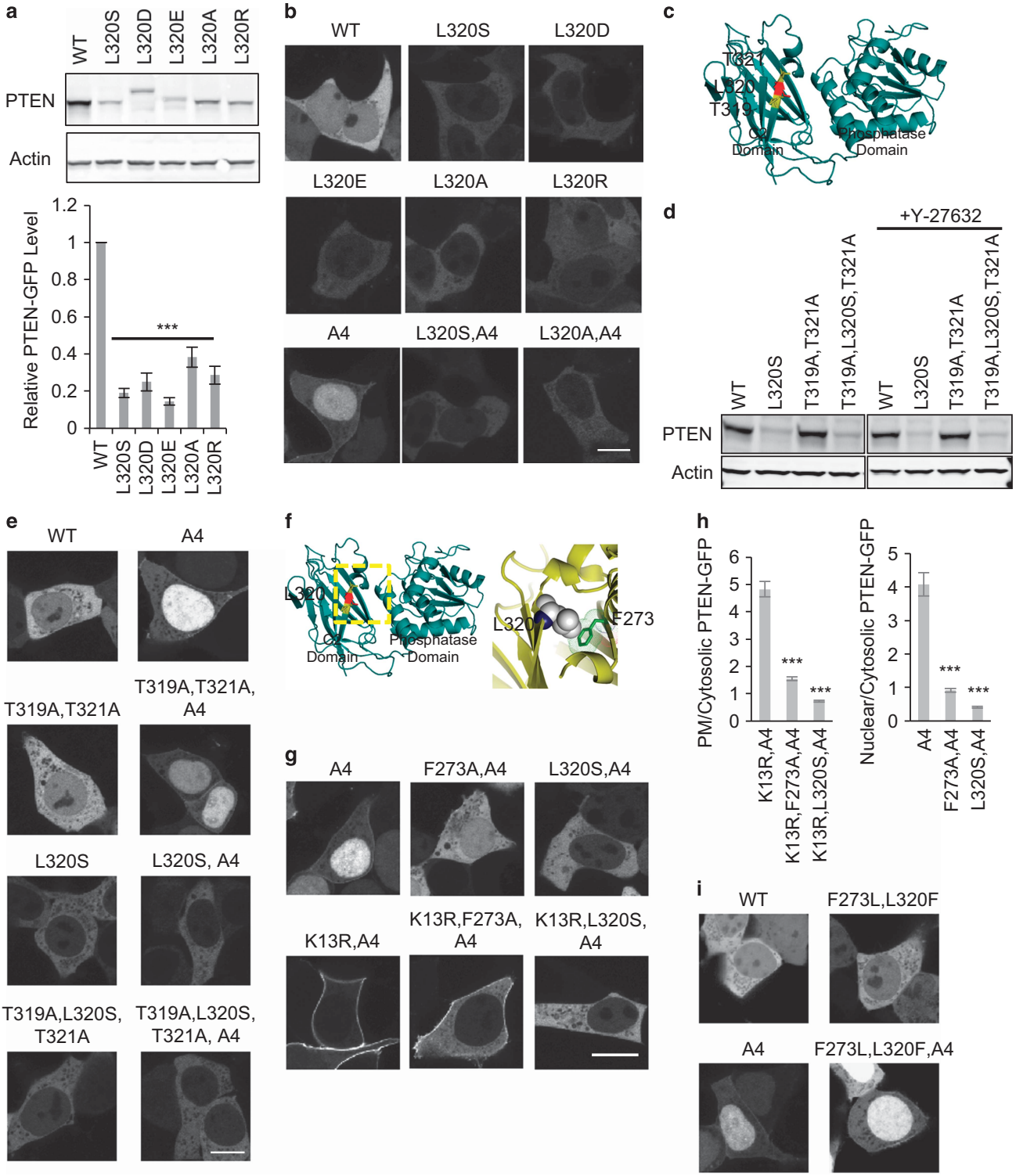

Figure 5. Mutational analysis of L320S. (**a, b**) HEK293T cells expressing the phospho-mimetic or phospho-defective $PTEN_{L320}$-GFP variants were analysed by immunoblotting (**a**) and fluorescence microscopy (**b**). In the former, band intensity was quantified. Values represent mean ± s.e.m. ($n = 3$). HEK293T cells carrying mutations near the L320S site (**c**) were examined for their steady state levels by immunoblotting (**d**) and for localization by fluorescence microscopy (**e**). (**f**) Mutational analysis of F273. F273 is close to L320 in the 3-D crystal structure.[35] (**g**) Using fluorescence microscopy, HEK293T cells carrying F273A mutations were compared to those carrying L320S mutations. (**h**) PTEN-GFP intensity was quantified relative to cytosol intensity at the membrane (PM/cytosolic) and nucleus (nuclear/cytosolic). Values represent mean ± s.e.m. ($n = 10$). (**i**) HEK293T cells expressing the indicated PTEN-GFP constructs were analysed by fluorescence microscopy.

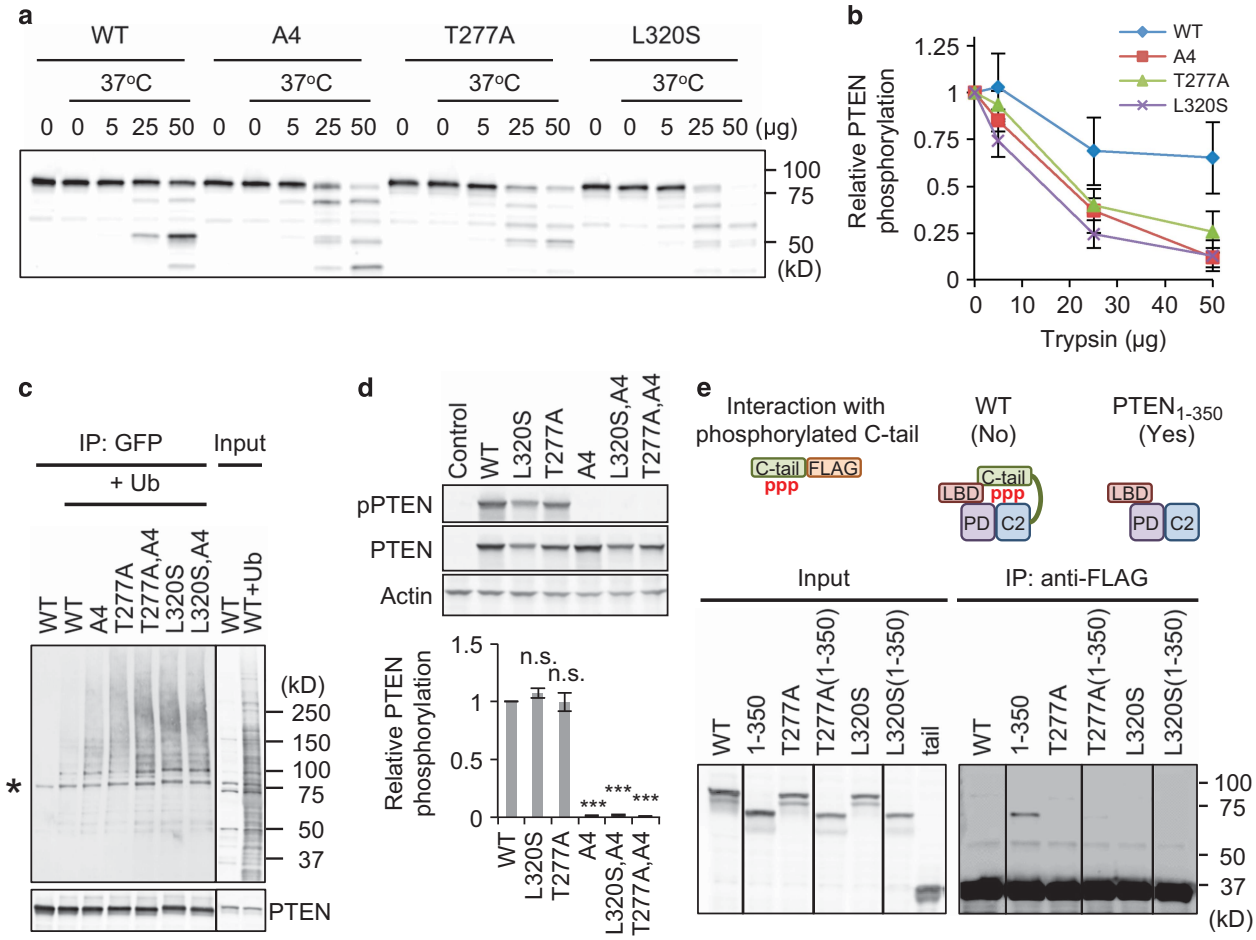

Figure 6. L320S and T277A open the conformation of PTEN. (**a**) PTEN-GFP proteins purified from HEK293T cells were incubated with trypsin for 10 min and analysed by immunoblotting with anti-PTEN antibodies. (**b**) Quantification of the band intensity of full-length PTEN-GFP. Values represent mean ± s.e.m. ($n = 4$). (**c**) The indicated GFP-PTEN proteins were expressed in HEK293T cells along with HA-ubiquitin and were immunoprecipitated using beads coupled to anti-GFP antibodies. The immunoprecipitated proteins were analysed by immunoblotting with antibodies to GFP and HA. (**d**) Phosphorylation of PTEN was quantitatively analysed by immunoblotting whole cell lysates carrying various PTEN constructs. Values represent mean ± s.e.m. ($n = 3$). (**e**) Whole-cell lysates from HEK293T cells expressing the indicated GFP-PTEN proteins were incubated with the C-terminal tail to create $PTEN_{352–403}$-YFP-FLAG, which was immunoprecipitated using beads coupled to anti-FLAG antibodies and analysed by immunoblotting.

elevate PTEN ubiquitination. We suggest that these elevated levels of ubiquitination likely account for protein instability in $PTEN_{A4}$, $PTEN_{T277A}$ and $PTEN_{L320S}$. In contrast, by immunoblotting whole cell lysates with anti-phospho-PTEN antibodies, we show that T277A and L320S do not change phosphorylation at the C-terminal tail, which is necessary for interaction with the membrane-binding regulatory interface (Figure 6d).

T277A and L320S inhibit the membrane-bound regulatory interface from interacting with the C-terminus

To further analyse the conformations of $PTEN_{T277A}$ and $PTEN_{L320S}$, we measured the intramolecular interaction between the membrane-binding regulatory interface and the phosphorylated C-terminal tail of PTEN.[37] In this assay, we mixed HEK293T cell lysates containing the PTEN C-terminal tail tagged with FLAG with those containing GFP-$PTEN_{WT}$, GFP-$PTEN_{T277A}$ or GFP-$PTEN_{L320S}$. Anti-FLAG agarose beads were added to the mixture to pull down the C-terminal tail-FLAG. We found that GFP-$PTEN_{WT}$, which has a closed conformation, did not co-precipitate with the tail, consistent with previous studies.[12,13] Similarly, GFP-$PTEN_{T277A}$ and GFP-$PTEN_{L320S}$ did not bind to the C-terminal tail-FLAG (Figure 6e). This could have resulted from either a closed conformation (a consequence of intramolecular interaction) or a loss in the ability of the membrane-binding regulatory interface to interact with the C-terminal tail. To distinguish between these mechanisms, we truncated the C-terminal tails from $PTEN_{T277A}$ and $PTEN_{L320S}$. We found that the truncated proteins, $PTEN(1\text{-}350)_{T277A}$ and $PTEN(1\text{-}350)_{L320S}$, were unable to bind to the C-terminal tail. These data suggest that $PTEN_{T277A}$ and $PTEN_{L320S}$ block interaction between the membrane-binding regulatory interface and the C-terminal tail (Figure 6e).

Rescuing nuclear localization defects of $PTEN_{T277A}$ and $PTEN_{L320S}$ using ubiquitin tagging

In addition to proteasome degradation, ubiquitination serves as a signal to drive the protein to the nucleus. We found that tagging $PTEN_{WT}$-GFP with ubiquitin at the C-terminus of PTEN enhances its nuclear localization (Figure 7a). We further tested the ability of the C-terminal ubiquitin tag to drive PTEN to the nucleus using $PTEN_{K13R,A4}$, which is almost completely excluded from the nucleus (Figures 7a and b). Surprisingly, we found a significant amount of $PTEN_{K13R,A4}$-Ub-GFP accumulated in the nucleus. Therefore, the C-terminal ubiquitin tag has a strong ability to drive PTEN to the nucleus.

We then tested whether the C-terminal ubiquitin tag can rescue the nuclear localization defect of $PTEN_{L320S}$. We found that

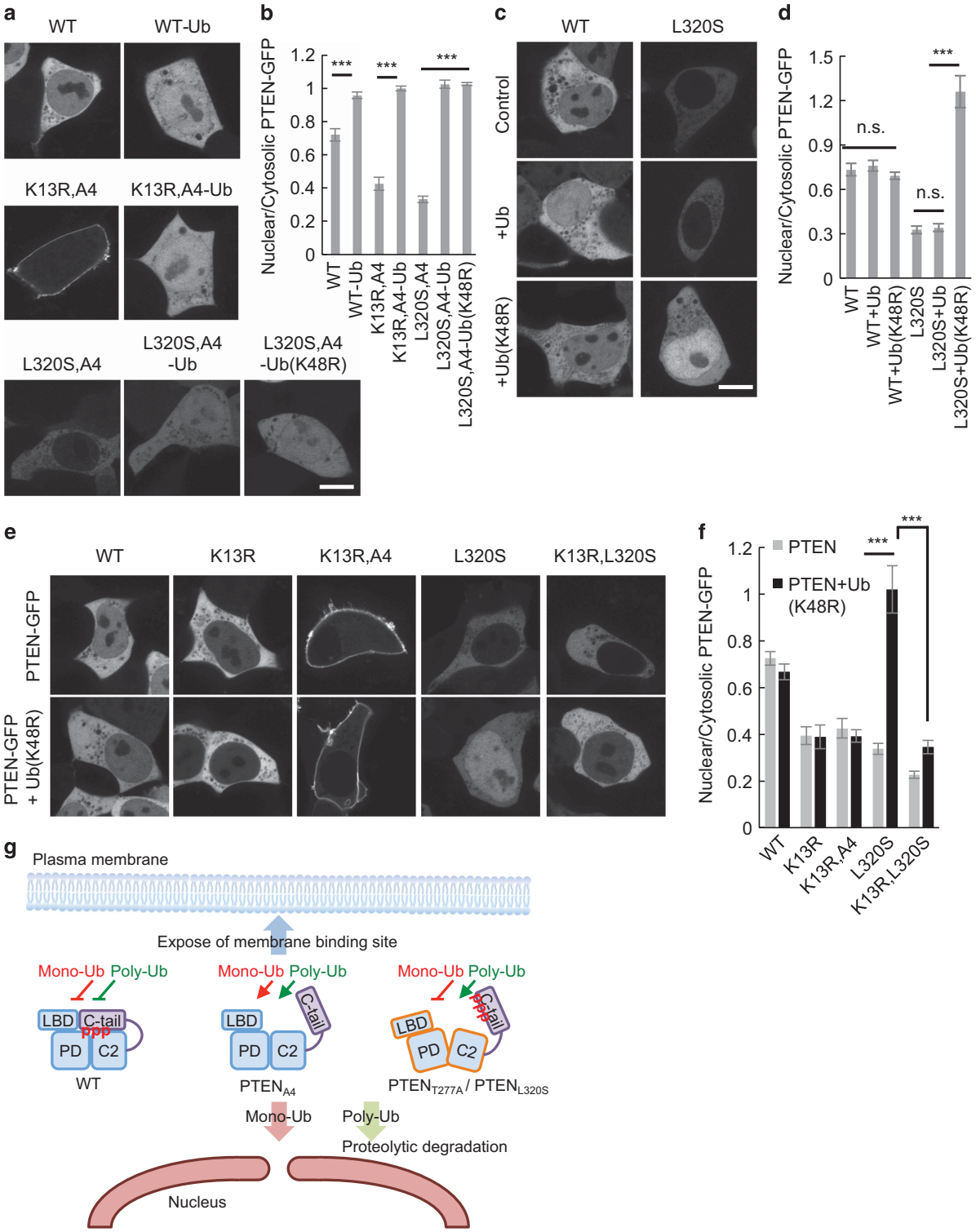

Figure 7. Mechanism of T277A and L320S mutations causing PTEN malfunction. (**a, b**) Fluorescence images (**a**) and quantification of nuclear localization (**b**) of PTEN in HEK293T cells expressing ubiquitin-tagged PTEN-GFP. Values represent mean ± s.e.m. ($n = 15$). (**c, d**) Fluorescence images and quantification of PTEN nuclear localization in HEK293T cells co-expressing variants of ubiquitin and PTEN-GFP. Values represent mean ± s.e.m. ($n = 15$). (**e**) HEK293T cells co-expressing the indicated PTEN and ubiquitin molecules were examined using fluorescence microscopy. (**f**) Quantification of PTEN accumulating at the plasma membrane. Values represent mean ± s.e.m. ($n = 15$). (**g**) T277A and L320S mutations alter PTEN conformation, which prohibits membrane association of PTEN through disruption of the membrane-interacting surface. These mutations also inhibit PTEN accumulation in the nucleus, possibly through reduced mono-ubiquitination. Mutant PTENs are subjected to accelerated degradation by enhanced poly-ubiquitination.

$PTEN_{L320S,A4}$-Ub-GFP significantly accumulated in the nucleus (Figures 7a and b). To determine whether polyubiquitination is required for this rescuing activity, we tested $ubiquitin_{K48R}$, which prevents the formation of polyubiquitin chains via Lys48 linkages. We found that $PTEN_{L320S,A4}$-Ub_{K48R}-GFP showed increased nuclear localization, showing that polyubiquitination is not required.

We also tested the effect of co-expression of $PTEN_{L320S}$-GFP and ubiquitin or $ubiquitin_{K48R}$ instead of expression of PTEN-ubiquitin fusion proteins. Intriguingly, in the presence of $ubiquitin_{K48R}$, $PTEN_{L320S}$-GFP showed strong nuclear accumulation (Figures 7c and d). This effect requires the K48R mutation because co-expression of ubiquitin did not affect the cytosolic localization of $PTEN_{L320S}$-GFP. Notably, no nuclear accumulation was observed when $PTEN_{WT}$-GFP was co-expressed with either ubiquitin or $ubiquitin_{K48R}$, supporting that the closed conformation of $PTEN_{WT}$ is resistant to ubiquitination. Furthermore, $ubiquitin_{K48R}$, but not ubiquitin, increased the abundance of $PTEN_{L320S}$-GFP, suggesting that the nuclear-targeting mono-ubiquitination decreases poly-ubiquitination, which drives the degradation of $PTEN_{L320S}$-GFP.

To determine if a lysine residue is necessary for the nuclear localization of PTEN on $ubiquitin_{K48R}$ expression, we tested lysine residues, K13, K254 and K289, and a cluster of five lysines (K260, K263, K266, K267, K269) in the CBR3 loop: these have been shown to undergo ubiquitination and sumoylation.[15,16,38,39] The substitution of K13 to arginine, but not other lysines, blocked the redistribution of $PTEN_{WT}$-GFP, $PTEN_{A4}$-GFP and $PTEN_{L320S}$-GFP to the nucleus (Figures 7e and f and Supplementary Figure S3).

DISCUSSION

In this study, we revealed that two GBM-associated mis-sense mutations in PTEN, $PTEN_{L320S}$ and $PTEN_{T277A}$, induce defects in the intracellular localization and protein stability of PTEN. They generate enzymatically active PTENs that are unable to down-regulate AKT signalling, leading to higher phospho-AKT levels and increased proliferation and migration in GBM than does wild-type PTEN. The mutated residues are located on opposite sides of the membrane-binding regulatory interface in the crystal structure of PTEN.[35] Importantly, these residues are located at the junction between the phosphatase and C2 domains, which together create the molecular surface critical for membrane localization and its regulation by the phosphorylated inhibitory C-terminal tail. One possible mechanism of blocking the interface is that the PTEN conformation is tightly closed as a result of intramolecular interactions between the interface and the phosphorylated inhibitory C-terminal tail. Unexpectedly, $PTEN_{L320S}$ and $PTEN_{T277A}$ are defective in this action because the membrane-binding regulatory interface is unable to associate with the C-terminal tail. At the same time, another key function of this interface (that is, interaction with the plasma membrane) is inhibited even though the inhibitory C-terminal tail is no longer masking this interface. This abnormally opened conformation increased polyubiquitination of PTEN and likely as a consequence of this, decreased the stability of PTEN. Polyubiquitination of PTEN controls its stability while its mono-ubiquitination and sumoylation have been suggested to regulate its nuclear localization.[16,29,30,40] We speculate that simultaneous effects on both localization and stability are major contributors to PTEN deficiency in GBM (Figure 7g). It should also be noted that $PTEN_{L320S}$ and $PTEN_{T277A}$ affect PIP3 signalling to various degrees. In this sense, it would be important to understand how this difference is created via structural analysis in future studies.

Our findings reveal that PTEN deficiency can be achieved by mutations at the junction between the phosphatase and C2 domains, inhibiting membrane and nuclear localization and enhancing protein degradation. To expand our findings to a larger perspective, we searched for mutations that are located at the same junction through the Catalogue of Somatic Mutations in Cancer (COSMIC) database: among 53 592 samples examined in this database, 3443 of them carry mutations in PTEN (6.4%), ~40% of which are mis-sense mutations that occur throughout the entire molecule with two hotspots, R130 and R173. First, we found that $PTEN_{T277}$ and $PTEN_{L320}$ are mutated in cancer patients in addition to those analysed in our current study (Supplementary Table S2). $PTEN_{T277}$ was mutated in endometrium carcinoma (T->A and T->R), lymphoid neoplasm (T->A) and glioma (T->I). $PTEN_{L320}$ was mutated in endometrium carcinoma (L->V). Second, in the vicinity of $PTEN_{T277}$ and $PTEN_{L320}$, there are additional amino acid residues in the C2 domain (amino acids 251–252, 270–278 and 325) that have been proposed to maintain the spatial configuration of the phosphatase and C2 domains based on the crystal structure. These residues are also mutated in different cancers and represent 27% of mis-sense mutations in the C2 domain (58 mutations/213 mutations in the C2 domain in COSMIC). The occurrence of these mutations at the junction indicates the importance of these residues in PTEN conformation, localization and function, and their alterations are commonly involved in the pathogenesis of a variety of cancers.

The identification of novel targets in GBM, a devastating brain cancer, is crucial to stop malignant cell proliferation and migration, and it will impact the survival in this patient population because personalized treatments are becoming more prevalent. In-depth analysis of PTEN mutation in GBM is necessary for designing personalized targeted therapies. A translation potential of our findings could entail the *in silico* design of specific inhibitors of polyubiquitination to enhance protein stability and restore normal intracellular localization.

MATERIALS AND METHODS

RT-PCR and cloning

The mRNA from each GBM cells was prepared using an RNeasy kit (Qiagen, Hilden, Germany) according to manufacturer's protocol. The PTEN cDNA was synthesized from mRNA using the following primer pair: 5′-ctggg atccaaataaaaATGACAGCCATCATCAAAGAGATCG-3′ and 5′-ctcctcgagccGA CTTTTGTAATTTGTGTATGCTGATCTTC-3′ using the OneStep RT-PCR kit (Qiagen). It was then amplified using the same primer pair with Phusion DNA polymerase (Thermo Fisher Scientific, Waltham, MA, USA). GAPDH was used as a control and was amplified using the primer pair 5′-ATGG GGAAGGTGAAGGTCGGA-3′ and 5′-TTACTCCTTGGAGGCCATGTGGG-3′. The PTEN cDNA from each GBM cell was cloned into a pCR-Blunt II-TOPO vector using a Zero Blunt TOPO PCR cloning kit (Life Technologies, Waltham, MA, USA). GFP was fused to the 3′-end of PTEN using overlapping PCR. It was then cloned into the pcDNA3.1-TOPO vector using the primer pair 5′-caccATGACAGCCATCATCAAAG-3′ and 5′-TTACTTGTACAGCTCGTCCATG-3′ through directional TOPO cloning (Life Technologies).

The plasmids and PCR primers used in this study are listed in Supplementary Table S1. PTEN variants were generated using overlapping extension PCR,[41] and they were cloned into either the mammalian expression vector pcDNA3.1 (Life Technologies), peGFP-C1 (Clontech, Mountain View, CA, USA), or the lentiviral vector pHR-SIN. All constructs were confirmed through DNA sequencing.

Cell culture and transfection

HEK293T cells were maintained in DMEM containing 10% FBS. Cells were transiently transfected with pcDNA3.1-PTEN-GFP or peGFP-C1-PTEN plasmids using Lipofectamine 3000 (Life Technologies) according to the manufacturer's protocol. Transfected cells were cultured overnight before analysis.

All protocols for GBM and human fetal cells were approved by the Johns Hopkins Hospital Institutional Review Board. All human brain tumour cells were derived from intraoperative tissue samples from patients treated surgically for newly diagnosed GBM at Johns Hopkins Hospital. Primary cultures of human fetal neural stem cells were derived after 18–20 weeks gestation, as previously published.[18–20] Detailed culture methodology, cell characterization and orthotropic tumour formation has been previously described.[23,24,42–46] Briefly, cells were cultured on laminin-coated dishes (1 $\mu g/cm^2$; L2020; Sigma, St Louis, MO, USA) in complete media (DMEM F/12 (Invitrogen 11330–032,

Waltham, MA, USA), Neuroplex serum-free supplement (Gemini 400–160, Sacramento, CA, USA), 20 ng/mL EGF and bFGF (Pepro Tech, Rocky Hill, NJ, USA) and an antibiotic/antimycotic (A5955; Sigma)). Cells were passaged upon reaching confluency using 0.05% trypsin/EDTA (Gibco-BRL, Waltham, MA, USA). Cell viability was evaluated using the automated Cell Viability Analyzer Vi-Cell XR (Beckman Coulter, Brea, CA, USA).

PTEN-expressing GBM cells were generated by lentivirus transduction. To make PTEN-GFP lentiviruses, HEK293T cells were transfected with three plasmids: pHR-SIN-PTEN-GFP, pCMV-VSVG and pCMV-ΔR8.2 using Lipofectamine 3000. Virus-containing media were added to GBM cells for transduction. Cells were analysed at least 3 days after transduction.

Phosphatase activity

The phosphatase activity of PTEN was measured as described previously (see Materials and methods section). GFP-tagged wild-type and mutant variants of PTEN were expressed in HEK293T cells and immunopurified using GFP-Trap beads (ChromoTek, Hauppauge, NY, USA). Enzymatic activity was determined by measuring the phosphate release rate from PIP3 diC8 using a malachite green phosphatase assay kit (Echelon, Salt Lake City, UT, USA). The activity was normalized relative to amounts of purified PTEN-GFP proteins.

Immunoblotting

Proteins were separated using SDS-PAGE and then were transferred onto PVDF membranes. Antibodies used were: PTEN (138G6; Cell Signaling, Danvers, MA, USA), phospho-PTEN (S380/T382/T383; #9549; Cell Signaling), GFP,[47–49] AKT (#9272; Cell Signaling), phospho-AKT (#4060; Cell Signaling), HA (12CA5), actin (C-11; Santa Cruz Biotechnology, Dallas, TX, USA), and GAPDH (sc-32233; Santa Cruz). Immunocomplexes were visualized using fluorescent-labelled secondary antibodies and detected using a PharosFX Plus molecular imager (Bio-Rad, Hercules, CA, USA).

Live-cell imaging

HEK293T cells were seeded in LabTek 8-well chambered slides (Nalge Nunc, Rochester, NY, USA) with phenol red-free DMEM medium (#21063-029; Gibco) supplemented with 10% FBS before transfection. Cells were transiently transfected with PTEN-GFP and RFP-PH_{AKT} plasmids using Lipofectamine 3000. After overnight incubation at 37 °C, cells were observed on a Zeiss LSM780-FCS laser scanning confocal microscope with Zen software (Zeiss, Oberkochen, Germany). Images were analysed using ImageJ (NIH).

Immunoprecipitation

Whole-cell lysates of HEK293T cells co-expressing HA-Ub and various PTEN-GFP constructs were prepared from 6-cm culture dishes containing 200 µl lysis buffer with deubiquitinase inhibitor NEM (20 mM Tris (pH 7.5), 150 mM NaCl, 0.5% NP-40, 20 mM NEM, 10% glycerol, 1 mM EDTA, protease inhibitor cocktail and phosphatase inhibitor cocktail). GFP-trap beads conjugated with anti-GFP antibodies were added to the lysates and incubated for 2 h at 4 °C. The beads were washed three times, and the bound proteins were analysed using SDS-PAGE, and immunoblotting was performed using antibodies against HA and PTEN.

Trypsin digestion assay

HEK293T cells were transiently transfected with pcDNA3.1-$PTEN_{WT}$-GFP, pcDNA3.1-$PTEN_{A4}$-GFP, pcDNA3.1-$PTEN_{T277A}$-GFP and pcDNA3.1-$PTEN_{L320S}$-GFP. Cell lysates were prepared with lysis buffer (20 mM Tris (pH 7.5), 150 mM NaCl, 0.5% NP-40, 10% glycerol, 1 mM EDTA, protease inhibitor cocktail and phosphatase inhibitor cocktail) and then incubated with GFP-trap beads to pull down GFP-tagged PTEN proteins. The beads were washed three times and then suspended in assay buffer (20 mM Tris (pH 7.5), 150 mM NaCl, 1 mM EDTA and 10 mM DTT). Trypsin digestion was performed by incubating various amounts of trypsin with the bead suspension at 37 °C for 10 min. Samples were analysed by immunoblotting with an anti-PTEN antibody.

Interactions between PTEN and its C-terminal tail

Association of PTEN with its C-terminal tail ($PTEN_{352\text{-}403}$-YFP-FLAG) was analysed as previously described.[22] Briefly, HEK293T cells were transiently transfected with plasmids carrying the PTEN C-terminal tail ($PTEN_{352\text{-}403}$-YFP-FLAG) or PTEN mutants. After overnight incubation, cells were lysed in lysis buffer (20 mM Tris (pH 7.5), 150 mM NaCl, 0.5% NP-40, 10% glycerol, 1 mM EDTA, protease inhibitor cocktail and phosphatase inhibitor cocktail). The lysates were then cleared by centrifugation at 13 000 rpm for 20 min at 4 °C. GFP-PTEN-containing lysates were mixed with $PTEN_{352\text{-}403}$-YFP-FLAG lysate at a 4:1 ratio, then 15 µl beads coupled to anti-FLAG antibodies (Sigma) were added. The lysate–bead mixture was incubated at 4 °C for 2 h. The bound fractions were analysed using SDS-PAGE and immunoblotting with antibodies to GFP, which recognize both GFP and YFP.

Transwell cell migration assay

GBM cells (2×10^4) expressing GFP or $PTEN_{WT}$-GFP were resuspended in 100 µl DMEM medium containing 0.5% FBS and then were seeded in 6.5-mm inserts with 8-µm pores (Transwell Permeable Support 3422, Corning, Corning, NY, USA), which were hung over a receiver well filled with 0.5 ml DMEM/F12 containing 2.5% FBS. The same volume was seeded in a separate well to determine the total number of cells seeded per insert. After 24 h incubation, the inside of each insert was gently wiped clean using cotton swabs to remove cells that did not transmigrate. The insert was placed under a Zeiss HAL100 epifluorescence inverted microscope, and the number of GFP-positive cells that transmigrated was counted from at least four random fields. The percentage of cells that migrated was calculated by dividing the total number of migrated cells expressing GFP by the total number of cells expressing GFP that were seeded per insert.

Nanopattern cell migration assay

Migration of glioma cells was quantified using a novel directional migration assay and a multi-well nanopatterned device constructed of transparent poly(urethane acrylate). Using UV-assisted capillary lithography, parallel nano-ridges and grooves 400 nm in width, 500 nm in depth and 400 nm apart were prepared as previously described.[23–25,50,51] Prior to plating, nanogrooved substrata were coated with poly-D-ornithine (10 µg/ml) for 15 min and then laminin (3 µg/cm^2) overnight. Cell migration was quantified using time-lapse microscopy with a motorized inverted microscope (IX81; Olympus, Center Valley, PA, USA) equipped with a Cascade 512B II CCD camera and a temperature- and gas-controlling environmental chamber. Phase-contrast and epi-fluorescence cell images were automatically recorded using Slidebook 4.1 (Intelligent Imaging Innovations, Denver, CO, USA) for 10 h at 10 min intervals.

A custom-made MATLAB script was used to calculate cell speed and persistence using time-lapse microscopy data.[23,24,43–46] Average speeds of individual cells were calculated from the total distance moved throughout the entire cell trajectory and the total time the cell was tracked. Persistence was obtained by calculating the ratio of the shortest distance between start and end points divided by the total distance moved.

Statistics

P values were calculated using the Student's *t*-test. $^*P < 0.05$; $^{**}P < 0.01$; $^{***}P < 0.005$.

CONFLICT OF INTEREST

The authors declare no conflict of interest.

ACKNOWLEDGEMENTS

This work was supported by NIH grants to Miho Iijima (GM084015), Hiromi Sesaki (GM089853) and Alfredo Quinones-Hinojosa (NS070024).

REFERENCES

1 Endersby R, Baker SJ. PTEN signaling in brain: neuropathology and tumorigenesis. *Oncogene* 2008; **27**: 5416–5430.
2 Li J, Yen C, Liaw D, Podsypanina K, Bose S, Wang SI *et al.* PTEN, a putative protein tyrosine phosphatase gene mutated in human brain, breast, and prostate cancer. *Science* 1997; **275**: 1943–1947.
3 Salmena L, Carracedo A, Pandolfi PP. Tenets of PTEN tumor suppression. *Cell* 2008; **133**: 403–414.
4 Ali IU, Schriml LM, Dean M. Mutational spectra of PTEN/MMAC1 gene: a tumor suppressor with lipid phosphatase activity. *J Natl Cancer Inst* 1999; **91**: 1922–1932.
5 Network CGAR, Comprehensive genomic characterization defines human glioblastoma genes and core pathways. *Nature* 2008; **455**: 1061–1068.

6 Riddick G, Fine HA. Integration and analysis of genome-scale data from gliomas. *Nat Rev Neurol* 2011; **7**: 439–450.
7 Ermoian RP, Furniss CS, Lamborn KR, Basila D, Berger MS, Gottschalk AR *et al.* Dysregulation of PTEN and protein kinase B is associated with glioma histology and patient survival. *Clin Cancer Res* 2002; **8**: 1100–1106.
8 Phillips HS, Kharbanda S, Chen R, Forrest WF, Soriano RH, Wu TD *et al.* Molecular subclasses of high-grade glioma predict prognosis, delineate a pattern of disease progression, and resemble stages in neurogenesis. *Cancer Cell* 2006; **9**: 157–173.
9 Chaichana KL, Chaichana KK, Olivi A, Weingart JD, Bennett R, Brem H *et al.* Surgical outcomes for older patients with glioblastoma multiforme: preoperative factors associated with decreased survival. Clinical article. *J Neurosurg* 2011; **114**: 587–594.
10 Chaichana KL, Jusue-Torres I, Navarro-Ramirez R, Raza SM, Pascual-Gallego M, Ibrahim A *et al.* Establishing percent resection and residual volume thresholds affecting survival and recurrence for patients with newly diagnosed intracranial glioblastoma. *Neuro Oncol* 2014; **16**: 113–122.
11 Stupp R, Mason WP, van den Bent MJ, Weller M, Fisher B, Taphoorn MJ *et al.* Radiotherapy plus concomitant and adjuvant temozolomide for glioblastoma. *N Engl J Med* 2005; **352**: 987–996.
12 Nguyen HN, Afkari Y, Senoo H, Sesaki H, Devreotes PN, Iijima M. Mechanism of human PTEN localization revealed by heterologous expression in Dictyostelium. *Oncogene* 2014; **33**: 5688–5696.
13 Nguyen HN, Yang JM, Afkari Y, Park BH, Sesaki H, Devreotes PN *et al.* Engineering ePTEN, an enhanced PTEN with increased tumor suppressor activities. *Proc Natl Acad Sci USA* 2014; **111**: E2684–E2693.
14 Nguyen HN, Yang Jr JM, Rahdar M, Keniry M, Swaney KF, Parsons R *et al.* A new class of cancer-associated PTEN mutations defined by membrane translocation defects. *Oncogene* 2015; **34**: 3737–3743.
15 Nguyen HN, Yang JM, Miyamoto T, Itoh K, Rho E, Zhang Q *et al.* Opening the conformation is a master switch for the dual localization and phosphatase activity of PTEN. *Sci Rep* 2015; **5**: 12600.
16 Trotman LC, Wang X, Alimonti A, Chen Z, Teruya-Feldstein J, Yang H *et al.* Ubiquitination regulates PTEN nuclear import and tumor suppression. *Cell* 2007; **128**: 141–156.
17 Guerrero-Cazares H, Gonzalez-Perez O, Soriano-Navarro M, Zamora-Berridi G, Garcia-Verdugo JM, Quinones-Hinojosa A. Cytoarchitecture of the lateral ganglionic eminence and rostral extension of the lateral ventricle in the human fetal brain. *J Comp Neurol* 2011; **519**: 1165–1180.
18 Levy AF, Zayats M, Guerrero-Cazares H, Quinones-Hinojosa A, Searson PC. Influence of basement membrane proteins and endothelial cell-derived factors on the morphology of human fetal-derived astrocytes in 2D. *PLoS One* 2014; **9**: e92165.
19 Ravin R, Blank PS, Steinkamp A, Rappaport SM, Ravin N, Bezrukov L *et al.* Shear forces during blast, not abrupt changes in pressure alone, generate calcium activity in human brain cells. *PLoS One* 2012; **7**: e39421.
20 Tzeng SY, Guerrero-Cazares H, Martinez EE, Sunshine JC, Quinones-Hinojosa A, Green JJ. Non-viral gene delivery nanoparticles based on poly(beta-amino esters) for treatment of glioblastoma. *Biomaterials* 2011; **32**: 5402–5410.
21 Zhu M, Feng Y, Dangelmajer S, Guerrero-Cazares H, Chaichana KL, Smith CL *et al.* Human cerebrospinal fluid regulates proliferation and migration of stem cells through insulin-like growth factor-1. *Stem Cells Dev* 2015; **24**: 160–171.
22 Yang JM, Nguyen HN, Sesaki H, Devreotes PN, Iijima M. Engineering PTEN function: membrane association and activity. *Methods* 2014; **77-78**: 119–124.
23 Abbadi S, Rodarte JJ, Abutaleb A, Lavell E, Smith CL, Ruff W *et al.* Glucose-6-phosphatase is a key metabolic regulator of glioblastoma invasion. *Mol Cancer Res* 2014; **12**: 1547–1559.
24 Smith CL, Chaichana KL, Lee YM, Lin B, Stanko KM, O'Donnell T *et al.* Pre-exposure of human adipose mesenchymal stem cells to soluble factors enhances their homing to brain cancer. *Stem Cells Transl Med* 2015; **4**: 239–251.
25 Smith CL, Kilic O, Schiapparelli P, Guerrero-Cazares H, Kim DH, Sedora-Roman NI *et al.* Migration phenotype of brain-cancer cells predicts patient outcomes. *Cell Rep* 2016; **15**: 2616–2624.
26 Papa A, Wan L, Bonora M, Salmena L, Song MS, Hobbs RM *et al.* Cancer-associated PTEN mutants act in a dominant-negative manner to suppress PTEN protein function. *Cell* 2014; **157**: 595–610.
27 Das S, Dixon JE, Cho W. Membrane-binding and activation mechanism of PTEN. *Proc Natl Acad Sci USA* 2003; **100**: 7491–7496.
28 Al-Khouri AM, Ma Y, Togo SH, Williams S, Mustelin T. Cooperative phosphorylation of the tumor suppressor phosphatase and tensin homologue (PTEN) by casein kinases and glycogen synthase kinase 3beta. *J Biol Chem* 2005; **280**: 35195–35202.
29 Maccario H, Perera NM, Davidson L, Downes CP, Leslie NR. PTEN is destabilized by phosphorylation on Thr366. *Biochem J* 2007; **405**: 439–444.
30 Bassi C, Ho J, Srikumar T, Dowling RJ, Gorrini C, Miller SJ *et al.* Nuclear PTEN controls DNA repair and sensitivity to genotoxic stress. *Science* 2013; **341**: 395–399.
31 Gil A, Andres-Pons A, Pulido R. Nuclear PTEN: a tale of many tails. *Cell Death Differ* 2007; **14**: 395–399.
32 Song MS, Carracedo A, Salmena L, Song SJ, Egia A, Malumbres M *et al.* Nuclear PTEN regulates the APC-CDH1 tumor-suppressive complex in a phosphatase-independent manner. *Cell* 2011; **144**: 187–199.
33 Kamimura Y, Xiong Y, Iglesias PA, Hoeller O, Bolourani P, Devreotes PN. PIP3-independent activation of TorC2 and PKB at the cell's leading edge mediates chemotaxis. *Curr Biol* 2008; **18**: 1034–1043.
34 Li Z, Dong X, Wang Z, Liu W, Deng N, Ding Y *et al.* Regulation of PTEN by Rho small GTPases. *Nat Cell Biol* 2005; **7**: 399–404.
35 Lee JO, Yang H, Georgescu MM, Di Cristofano A, Maehama T, Shi Y *et al.* Crystal structure of the PTEN tumor suppressor: implications for its phosphoinositide phosphatase activity and membrane association. *Cell* 1999; **99**: 323–334.
36 Bolduc D, Rahdar M, Tu-Sekine B, Sivakumaren SC, Raben D, Amzel LM *et al.* Phosphorylation-mediated PTEN conformational closure and deactivation revealed with protein semisynthesis. *Elife* 2013; **2**: e00691.
37 Yang JM, Nguyen HN, Sesaki H, Devreotes PN, Iijima M. Engineering PTEN function: membrane association and activity. *Methods* 2015; **77-78**: 119–124.
38 Lang V, Aillet F, Da Silva-Ferrada E, Xolalpa W, Zabaleta L, Rivas C *et al.* Analysis of PTEN ubiquitylation and SUMOylation using molecular traps. *Methods* 2015; **77–78**: 112–118.
39 Liu F, Wagner S, Campbell RB, Nickerson JA, Schiffer CA, Ross AH. PTEN enters the nucleus by diffusion. *J Cell Biochem* 2005; **96**: 221–234.
40 Wang X, Shi Y, Wang J, Huang G, Jiang X. Crucial role of the C-terminus of PTEN in antagonizing NEDD4-1-mediated PTEN ubiquitination and degradation. *Biochem J* 2008; **414**: 221–229.
41 Zhang P, Wang Y, Sesaki H, Iijima M. Proteomic identification of phosphatidylinositol (3,4,5) triphosphate-binding proteins in *Dictyostelium discoideum*. *Proc Natl Acad Sci USA* 2010.
42 Chaichana KL, Guerrero-Cazares H, Capilla-Gonzalez V, Zamora-Berridi G, Achanta P, Gonzalez-Perez O *et al.* Intra-operatively obtained human tissue: protocols and techniques for the study of neural stem cells. *J Neurosci Methods* 2009; **180**: 116–125.
43 Feng Y, Zhu M, Dangelmajer S, Lee YM, Wijesekera O, Castellanos CX *et al.* Hypoxia-cultured human adipose-derived mesenchymal stem cells are non-oncogenic and have enhanced viability, motility, and tropism to brain cancer. *Cell Death Dis* 2014; **5**: e1567.
44 Garzon-Muvdi T, Schiapparelli P, ap Rhys C, Guerrero-Cazares H, Smith C, Kim DH *et al.* Regulation of brain tumor dispersal by NKCC1 through a novel role in focal adhesion regulation. *PLoS Biol* 2012; **10**: e1001320.
45 Kondapalli KC, Llongueras JP, Capilla-Gonzalez V, Prasad H, Hack A, Smith C *et al.* A leak pathway for luminal protons in endosomes drives oncogenic signalling in glioblastoma. *Nat Commun* 2015; **6**: 6289.
46 Li Q, Wijesekera O, Salas SJ, Wang JY, Zhu M, Aprhys C *et al.* Mesenchymal stem cells from human fat engineered to secrete BMP4 are nononcogenic, suppress brain cancer, and prolong survival. *Clin Cancer Res* 2014; **20**: 2375–2387.
47 Chen CL, Wang Y, Sesaki H, Iijima M. Myosin I links PIP3 signaling to remodeling of the actin cytoskeleton in chemotaxis. *Sci Signal* 2012; **5**: ra10.
48 Wang Y, Steimle PA, Ren Y, Ross CA, Robinson DN, Egelhoff TT *et al. Dictyostelium huntingtin* controls chemotaxis and cytokinesis through the regulation of myosin II phosphorylation. *Mol Biol Cell* 2011; **22**: 2270–2281.
49 Zhang P, Wang Y, Sesaki H, Iijima M. Proteomic identification of phosphatidylinositol (3,4,5) triphosphate-binding proteins in *Dictyostelium discoideum*. *Proc Natl Acad Sci USA* 2010; **107**: 11829–11834.
50 Kim DH, Han K, Gupta K, Kwon KW, Suh KY, Levchenko A. Mechanosensitivity of fibroblast cell shape and movement to anisotropic substratum topography gradients. *Biomaterials* 2009; **30**: 5433–5444.
51 Kim DH, Seo CH, Han K, Kwon KW, Levchenko A, Suh KY. Guided cell migration on microtextured substrates with variable local density and anisotropy. *Adv Funct Mater* 2009; **19**: 1579–1586.

Supplementary Information accompanies this paper on the Oncogene website (http://www.nature.com/onc)